Materials Today Bio 28 (2024) 101207

Contents lists available at ScienceDirect

Materials Today Bio

journal homepage: www.journals.elsevier.com/materials-today-bio

Combinatory electric-field-guided deposition for spatial microparticles patterning

Zhiyuan Zheng [a], Yang Zhang [a,b], Jinyu Xing [c], Xin Li [d,e], Zhiqiang Zhu [a], Min Ye [d,e,**], Shuwei Shen [d,e,*], Ronald X. Xu [a,d,e,***]

[a] Department of Precision Machinery and Precision Instrumentation, University of Science and Technology of China, Hefei, 230026, China
[b] Department of Rehabilitation Medicine, The First Affiliated Hospital of USTC, Division of Life Sciences and Medicine, University of Science and Technology of China, Hefei, Anhui, 230001, China
[c] Institute of Advanced Technology, University of Science and Technology of China, Hefei, 230026, China
[d] School of Biomedical Engineering, Division of Life Sciences and Medicine, University of Science and Technology of China, Hefei, Anhui, 230026, China
[e] Suzhou Institute for Advanced Research, University of Science and Technology of China, Suzhou, 215000, China

ARTICLE INFO

Keywords:
Electrospray
Microparticle deposition
Electric field
Pattern

ABSTRACT

Spatial deposition and patterning of microparticles are crucial in chemistry, medicine, and biology. Existing technologies like electric force manipulation, despite precise trajectory control, struggle with complex and personalized patterns. Key challenges include adjusting the quantity of particles deposited in different areas and accurately depositing particles in non-continuous patterns. Here, we present a rational process termed combinatory electric-field-guided deposition (CED) for achieving spatially regulated microparticle deposition on insulative substrates. This process involves coating the substrates with insulating materials like PVP and positioning it on a relief-patterned negative electrode. The negative electric field generated by the electrode attracts microparticles, while the positive surface charges on the substrates repel microparticles, resulting in the formation of a potential well over the electrode area. Consequently, this configuration enables precise control over microparticle deposition without the need for direct contact with the substrate's surface, simplifying the process of switching masks to meet varying microparticle deposition requirements. Furthermore, we demonstrate the customization of patterned microparticles on superhydrophobic coatings to regulate cell distribution, as well as the successful loading of drug-laden microparticles onto antibacterial bandages to match the areas of skin lesions. These applications underscore the versatility of CED across chemical, medical, and bioengineering domains.

1. Introduction

Spatial deposition and patterning of microparticles have attracted more and more research interests in a wide range of fields, such as chemical, medical, and biological applications [1–4]. The manipulation of particles may be accomplished by an acoustic wave, electric force, capillary force, and many other effects [5–8]. Among these, electric-force manipulation has garnered significant interest due to its precision in controlling the trajectories of millions of particles simultaneously [9,10].

Over the years, numerous techniques have been developed to leverage electrostatic fields for selective deposition on substrate surfaces. Substrates can be directly designed into the desired pattern, allowing charged particles to be guided and deposited onto specific areas of the substrate via the electric field. A. Winkleman et al. demonstrated the self-assembly of 100 μm spheres on a patterned electrode under the guidance of an electric field [11]. Dielectrophoresis (DEP) offers another approach, manipulating particles based on the

* Corresponding author. School of Biomedical Engineering, Division of Life Sciences and Medicine, University of Science and Technology of China, Hefei, Anhui, 230026, China.
** Corresponding author. School of Biomedical Engineering, Division of Life Sciences and Medicine, University of Science and Technology of China, Hefei, Anhui, 230026, China.
*** Corresponding author. Department of Precision Machinery and Precision Instrumentation, University of Science and Technology of China, Hefei, 230026, China.
E-mail addresses: min_ye@ustc.edu.cn (M. Ye), swshen@ustc.edu.cn (S. Shen), xux@ustc.edu.cn (R.X. Xu).

https://doi.org/10.1016/j.mtbio.2024.101207
Received 4 June 2024; Received in revised form 19 August 2024; Accepted 23 August 2024
Available online 30 August 2024

contrast between the polarizabilities of the particles and the liquid medium [12]. Additionally, when substrates cannot be patterned as required directly, stencils or masks become indispensable tools. They not only prevent particles from depositing on undesired surfaces [13,14], but also assist in creating complex particle patterns by physically blocking the particles' trajectory while adjusting the electric field to modify their paths [15].

Despite significant advancements, current electric-field-based deposition techniques still face notable limitations, particularly in deploying complex and personalized patterns. These methods generally employ electrodes as equipotential bodies, which create a uniform attraction across all areas, consequently limiting the precision with which particle quantities can be controlled during a single deposition step [16–21]. Additionally, the inability to separate process control from the material properties—such as viscosity—means that the deposition process is inherently influenced by the surface characteristics of the materials being coated. This dependence not only complicates maintaining clean and sterile conditions but also presents challenges in fields such as precision medicine and tissue engineering, where custom treatments and biomimetic structures are essential. Moreover, the creation of non-continuous designs, such as isolated islands [22] or intricate shapes, requires regulated connections between all parts to circumvent complex alignment processes. These patterns have been widely adopted for many structural fabrications, such as microfluidic channels [23] and stamps for micro-contact printing [24,25].

To address these challenges, we introduce the Combinatory Electric-field-guided Deposition (CED) method, an approach that leverages a combinatory electric field to enable precise, programmable microparticle deposition on various substrates. Our method is distinct in its ability to adjust the electrical properties dynamically, allowing for complex pattern integrations without the need for physical masks or alignment processes. The CED process regulates the charged particles produced by electrospray using a combinatory electric field that derives from a positively charged insulative substrate and a negatively charged anode beneath the substrate. The negative electric field (NEF) generated by the negatively connected electrode attracts particles, while the positive electric field (PEF) generated by the positive surface charges repels particles. The interaction between NEF and PEF creates a potential well that directs the deposition of particles onto the Electrode Mapping Region (EMR), which is the top surface of the substrate directly above the electrode pattern, as illustrated in Fig. 1(a). By varying the electrical properties of different electrode areas, rather than using electrodes as equipotential bodies, the field strength can be tailored, enabling precise control over the quantity of particles deposited. Additionally, with the electrodes positioned beneath the substrate, its surface characteristics do not affect the deposition process. This design also allows for the use of electrode patterns of any complexity without impacting deposition. This research aims to significantly advance the capabilities of microparticle deposition technologies, offering new possibilities for applications in precision medicine, tissue engineering, and beyond.

2. Materials and methods

2.1. Materials

Coumarin 6, Rhodamine B, Phosphate buffered saline (PBS), ethyl acetate, Polyvinyl pyrrolidone (PVP, K30), acetone, and curcumin were purchased from Sino Pharm Chemical Reagent Co., Ltd. (Shanghai, China). Shipley S1813 photoresist and its developer MF-319 were purchased from MicroChem Corp. (MA, USA). Poly(lactic-co-glycolic acid) (PLGA, 50:50, Mw = 10 kDa) was obtained from Shandong Institute of Medical Instrument (Shandong, China). P. aeruginosa ATCC 15692 (PAO1) was purchased from American Type Culture Collection (ATCC). Luria-Bertani broth (LB broth) and LB agar plates were obtained by Yasong Biotechnology Co., Ltd. (Nanjing, China). Positive charge-treated glass slides (188105W) and untreated glass slides (10127105P)

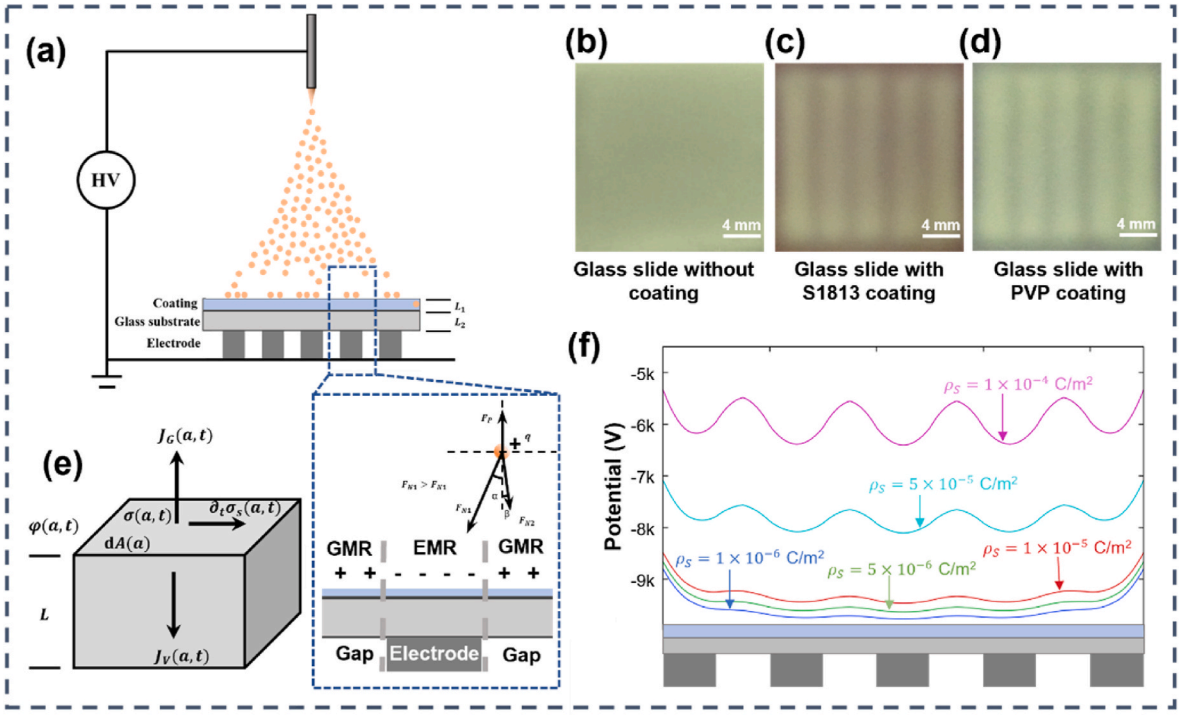

Fig. 1. Selective deposition of charged microparticles produced by electrospray under CED. (a) Schematic representation showing the impact of electrospray microparticles on the charge distribution on the substrate coating surface and their deposition under CED guidance. The impact of various surface coatings on the patterned deposition of particles on a glass substrate is shown under stripe electrode guidance, with microparticles deposited on uncoated (b), photoresist S1813 coated (c), and PVP coated (d) glass substrates. (e) Illustration of three pathways for surface charge dissipation on the substrate. (f) COMSOL simulations demonstrating the effects of surface charge density on the electrical potential distribution across a substrate with a thickness of 1 mm.

were purchased from Citotest Experimental Equipment Co., Ltd. (Jiangsu, China). PLA filament for 3D printing was purchased from Shenzhen JGAurora Co., Ltd. FH1100 resin for 3D printing was purchased from Zhejiang Flashforge 3D Technology Co., Ltd. (Zhejiang, China). HFL-301W resin was purchased from Anhui Zhongjian 3D Technology Co., Ltd. (Anhui, China). Deionized water (DI water) was produced by a pure infinity water purification system (Barnstead International, Dubuque, USA). Other materials purchased from Sigma-Aldrich (Darmstadt, Germany). The permittivity and conductivity of materials were measured using an IM 3570 impedance analyzer (HIOKI E.E. Co., Ltd., Nagano, Japan). The surface charge of substrates was measured using a Faraday cage (Shenzhen Huace Co., Ltd., Guangdong China).

2.2. Electrode fabrication

The conductive electrodes were processed with copper, aluminum, and structural steel using Haas DM-1 computer numerical control (CNC) machine (California, USA). The insulative electrodes were fabricated using JGAurora A6 3D printer (Guangdong, China) and Flashforge Hunter 3D printer (Zhejiang, China). All cubic electrodes were fabricated from a 15 mm × 15 mm × 15 mm 3D model. Besides, a cube-like electrode with a stripe pattern was fabricated with copper using the CNC machine.

2.3. Electrospray setup

The electrospray (ES) system consisted of a particle generation module and a process monitoring module (Fig. 1(a)), similar to our previous experimental setup. The particle generation module was composed of an 18G stainless-steel needle, a syringe pump (Pump 11, Harvard Apparatus, MA, USA), a substrate, an electrode, and two high-voltage DC power supplies (positive and negative voltages, Gamma High Voltage Research, Inc., FL, USA). The process monitoring module consisted of a charge-coupled device camera (Allied Vision Technologies, Inc., MA, USA), a computer, and a microscopic lens (Model VT-7DS-2CD, Hangzhou, China).

The ES solution was prepared by dissolving PLGA in acetone at a ratio of 5 % (w/v). Coumarin 6 or rhodamine B was also added into the solution at a ratio of 0.1 % (w/v) for observation. The solution was pumped through the needle by the syringe pump at a flow rate of 1 $mL \bullet h^{-1}$. The applied voltage was set as 7.5 kV for the positive end and 2–8 kV for the negative end to achieve a stable Taylor cone during the ES process. The electrode was connected with the negative end and the substrate was positioned upon the electrode.

2.4. Fabrication of glass substrate surface coating

To explore the preparation methods of photoresist coatings, clean glass substrates are placed on a spin coater, carefully covered with S1813 photoresist, and spun at 500 rpm for 1 min. The substrates are then baked on a hot plate at 105 °C for 1 min to form the photoresist coating. The PVP coating process involves preparing aqueous PVP solutions at concentrations of 12.5 %, 25 %, 37.5 %, 50 %, and 62.5 % (w/v). These solutions are carefully applied to clean glass substrates and spun at 2000 rpm for 1 min, followed by baking at 30 °C for 30 min to achieve varying thicknesses. The thickness of each coating is measured using SEM by observing the cross-sections.

2.5. Pre-patterning of photoresist

The S1813 was used to determine the difference of dissolved photoresist between pre-patterned and uniform deposited photoresist layers. First, the S1813 was dissolved in acetone in a volume ratio of 50 % for particle deposition using electrospray with or without patterned electrode guidance. After deposition, both S1813 layers were exposed with the same mask. For the patterned electrode-guided one, the mask was aligned with the pattern to cover the electrode region. Then, the exposed samples were rinsed with two 50 mL MF-319 solutions, respectively. Finally, the two solutions were diluted 10 times to determine the concentration of S1813 in the solution using a UV–Vis spectrophotometer (UNICO Instrument Co., Ltd., Shanghai, China). The measurement of S1813 concentration was repeated for 5 times.

2.6. Cell culture and adhesion

EA.hy926 endothelial cells (EA.hy926) were sourced from the Cell Bank of the Typical Culture Collection at the Chinese Academy of Sciences in Shanghai, China. These cells were cultured in DMEM medium containing 4.5 g/L glucose, supplemented with 10 % FBS, 100 U/mL benzylpenicillin, 100 μg/mL streptomycin, and 2 mM L-glutamine. Culturing conditions were maintained at 37 °C in a 5 % CO2 incubator. For the experiments, cells from passage number 5 were used to ensure consistency and reliability in experimental outcomes.

To control cell adhesion, a patterned distribution of particles was created on the surface of glass slides. One side of the slides was immersed in a 0.2 % (v/v) Pluronic F127 (F127) solution for 3 h to establish a surface coating. After removal, the slides were dried and washed three times with phosphate-buffered saline (PBS). PLGA microspheres were then selectively deposited on the F127-coated side by CED. Finally, the substrates were placed in 6-well plates and exposed to ultraviolet radiation for 60 min for sterilization. Subsequently, 2 ml of a cell suspension containing EA.hy926 endothelial cells (EA.hy926) (1 × 104/cm2) was carefully dispensed into each well. After overnight(12h) seeding, the glass substrates were gently rinsed with PBS to remove any unattached cells.

2.7. Immunofluorescent staining

The samples were initially rinsed with PBS to eliminate any detached and dead cells. Subsequently, the cells were fixed using 4 % formaldehyde for 30 min and then permeabilized with 0.5 % Triton-X-100 for 10 min at room temperature to prepare them for staining. Next, the cells were incubated in a blocking solution composed of 0.1 % Triton X-100 and 3 % bovine serum albumin (BSA) for 30 min to prevent non-specific staining. After a final wash with PBS, the cellular skeleton and nuclei were simultaneously stained with Propidium Iodide (Selleckchem, Texas, United States) and Phalloidin-iFluor 647 (Abcam, Cambridge, UK) respectively, for 20 min at room temperature, highlighting the cellular structure and nuclei for subsequent microscopic analysis.

2.8. In vitro drug release

An *in vitro* drug release test was carried out for curcumin-loaded PLGA particles within different regions after deposition. The 5 % (w/v) curcumin and 5 % (w/v) PLGA acetone solution were used for PLGA particle deposition onto a medical bandage under the guidance of a circular electrode with 2 mm in diameter. After deposition, the bandage was cut into two pieces according to the inner and outer electrode regions with a 2 mm-diameter punch. Finally, the two pieces were rinsed into 100 mL PBS solutions with pH = 7.4 for release test under 37 °C, respectively. At the scheduled time interval of 0, 1, 2, 4, 6, 9, 12, 24, 36, and 48 h, 100 μL solutions were sampled to determine the concentration of curcumin using the UV–Vis spectrophotometer. The *in vitro* drug release test was repeated 3 times for each group.

2.9. Antibacterial properties of bandage

The bacteria (PAO1) suspensions were shaken at 37 °C for 3 h before sampling. Then, sampled suspensions were diluted to 105 colony-forming units per milliliter (CFU/mL). The 5 % (w/v) curcumin and 5 % (w/v) PLGA acetone solution were used for PLGA particle deposition

onto a medical bandage under the guidance of a circular electrode with 2 mm in diameter. The prepared bandage was punched into two pieces according to the inner and outer electrode regions with a 2 mm-diameter punch. Then, the two pieces were soaked in the bacterial solution and shaken at 37 °C for 12 h, respectively. Finally, 100 mL of the solution was seeded in the LB agar plate. Quantification of the viability was conducted after 12h of incubation at 37 °C by CFU counting. The CFU was measured based on 3 individual samples for each group.

2.10. Characterization of electrosprayed particles

The optical and fluorescent images were acquired using a fluorescent microscope (Nikon Eclipse LV 100, Tokyo, Japan) with a FITC filter. The fluorescent intensity of fluorescent images was measured using the Advanced Research Nikon Elements Imaging Software (AR-NIS, Nikon). The edge gradient was measured based on the fluorescent images. The particle numbers were calculated using the ImageJ software based on 3 individual samples for each electrode. For each sample, 3 images were taken for calculation with a window of 317.44 μm × 317.44 μm in size. The measurement of surface charge was repeated for 5 times. The cross-stripe sample in red and green colors was processed using MATLAB 2019a software to obtain red and green channel images. The gray value of stripes in each channel image was calculated based on all 5 stripes using the ImageJ software. This measurement was performed for 3 times with 3 individual samples. The morphologic characteristics of electrosprayed particles were observed by the scanning electron microscope (SEM) (FESEM, UltraPlus, Zeiss). The SEM was operated at +10 kV in high vacuum mode, and the MNs underwent a gold-coating process before SEM imaging.

2.11. Statistical analysis

Student's *t*-test was used to examine whether there were significant differences in the particle number variation with different electrodes. The impacts of the electrode properties on particle number were analyzed using one-way ANOVA. Statistical analyses were performed using JMP 11.0 (SAS®, NC, USA). $p < 0.05$ (*) was considered significant and $p < 0.01$ (**) was considered highly significant.

3. Results and discussion

3.1. Combinatory electric-field-guided deposition by electrospray

In a typical electrospray process, microparticles are produced when a polymer solution is supplied to a capillary needle at a constant flow rate by a syringe pump and charged in a high-voltage electric field. When the electric force overcomes the surface tension at the needle tip, a cone-shaped structure known as a Taylor cone forms. The positively charged polymer droplets are then drawn toward the collector by electric forces and gravity. The electrostatic field, particularly near the negative electrode, plays a crucial role in guiding this deposition process. As the droplets travel toward the collector, the solvent evaporates quickly, allowing the polymer chains to entangle and solidify into microparticles. By moving from high potential to low potential in the electric field, the charged droplets are effectively guided to form solid particles on the collector as their solvent evaporates.

When the substrate is positioned above the patterned electrode, particles settle uniformly across its surface, as shown in Fig. 1(b). However, when a coating such as photoresist or PVP is applied to the glass substrate through spin-coating (Fig. S1), the particles organize into patterns that mirror the underlying electrode, as shown in Fig. 1(c) and (d). This behavior is likely due to the accumulation of surface charges on the substrate, which alters the electric field distribution and guides the patterned deposition of the microparticles.

Microparticles generated by electrospray carry a substantial amount of positive charge, which accumulates on the receiving substrate as microparticles deposit and gradually dissipate over time. In an open circuit configuration in air, charges accumulating on the surface of an insulating substrate dissipate primarily by three pathways: bulk neutralization, air neutralization, and surface conduction [26], as shown in Fig. 1(e). Bulk neutralization refers to the process where charges dissipate through transfer to the substrate [27,28]. Air neutralization involves the interaction of charges with ions in the surrounding air [29], and surface conduction refers to the process of charge movement along the gas-solid interface [30]. We utilize the equation proposed by Zhang Boya and Zhang Guixin in their study to describe a theoretical model for the dissipation of surface charges [26].

$$\partial_t \sigma(a,t) = J_V(a,t) + J_G(a,t) + \partial_t \sigma_s(a,t) \tag{1}$$

where, $\sigma(a,t)$ represents the instantaneous surface charge density at the position a at time t, $J_V(a,t)$ denotes the charge dissipation through bulk neutralization, $J_G(a,t)$ reflects the charge dissipation through air neutralization, and $\partial_t \sigma_s(a,t)$ is the charge dissipation through surface conduction. In the absence of external ion sources, air neutralization is primarily caused by free ions generated from natural background radiation, hence making $J_G(a,t)$ independent of the substrate. Surface conduction primarily plays a significant role in environments with high humidity [31,32]. The current density for bulk neutralization, $J_V(a,t)$ can be expressed as:

$$J_V(a,t) = \frac{E}{K} + \frac{\partial D}{\partial t} = \frac{\varphi(a,t)}{L}\frac{1}{K} + \frac{\varepsilon}{L}\frac{\partial \varphi(a,t)}{\partial t} \tag{2}$$

where, E and D represent the electric field strength and electric displacement field at position a along the thickness direction of the insulating substrate, respectively. K is the resistivity of the insulating substrate, $\varphi(a,t)$ is the electric potential difference at position a, and L is the thickness of the insulating substrate. From this equation (2), it is evident that the greater the substrate resistivity K and the smaller the dielectric constant ε, the smaller $J_V(a,t)$ is. In fact, during the electrostatic atomization process, the surface charge density on the substrate quickly reaches a limit, after which the surface potential on the substrate remains essentially constant, while the potential on the underside of the substrate are provided and maintained constant by the negative electrode [32]. Therefore, the change in $\varphi(a,t)$ over time can be neglected. Thus, the above equation (2) can be simplified to:

$$J_V(a,t) = \frac{\varphi(a,t)}{L}\frac{1}{K}K \tag{3}$$

Furthermore, the charge dissipation through the bulk neutralization process plays a dominant role in the accumulation of surface charges on the substrate. As shown in Fig. 1(a), when the substrate surface has a coating, equation (3) can be further written as:

$$J_V(a,t) = \frac{\varphi(a,t)}{K_1 L_1 + K_2 L_2} \tag{4}$$

where, K_1 , L_1, K_2, and L_2 respectively represent the resistivity and thickness of the coating and the glass substrate. From this equation, it is evident that the presence of an insulating coating reduces the current density of bulk neutralization, thus the surface charge density on the substrate is higher than in the uncoated substrate. The rate of charge dissipation on a glass substrate is higher than that on a photoresist coating, leading to a faster accumulation of charge on the surface of the photoresist. This creates a focused electric field between the photoresist and the glass substrate, guiding the subsequent deposition of particles toward the glass substrate.

According to the above results, positively charged particles can be fabricated and deposited using combinatory electric-field-guided deposition (CED), forming a pattern identical to the electrode, as shown in Fig. 1(a). The deposition of particles is controlled by the positive electrostatic field (PEF) generated by the positive surface charge and the negative electrostatic field (NEF) generated by the negative electrode.

When the substrate is not charged, the NEF decreases dramatically crossing the insulative substrate, which weakens the influence of NEF on particle motion. However, when the substrate is positively charged, the generated PEF repels particles to land on the surface. The NEF couples with the PEF, forming a potential well above the negative electrode, which attracts particles to land on this region. Moreover, both the repelling of the out-electrode region and the attracting of the electrode region influence the particle motion, which finally leads the particles to form a pattern according to the electrode.

To verify the hypothesis, COMSOL is used to simulate the electric field distribution. The electric field is calculated by solving the Laplace equations [15]:

$$\nabla^2\Phi = \frac{\partial^2\Phi}{\partial x^2} + \frac{\partial^2\Phi}{\partial y^2} + \frac{\partial^2\Phi}{\partial z^2} = 0 \tag{5}$$

$$\mathbf{E} = -\nabla\Phi \tag{6}$$

By comparing Fig. 1(f), it is evident that the surface charge significantly enhances the aggregation of electric field lines from out-electrode region to electrode region. The presence of surface charges on the substrate enhances the potential difference between electrode mapping region (EMR) and gap mapping region (GMR), and this enhancement effect increases with the surface charge density. When the surface charge density reaches 5×10^{-5} C/m^2, the potential difference between EMR and GMR approaches 500 V. As the surface charge density continues to increase to 1×10^{-4} C/m^2, the potential difference between EMR and GMR approaches 1000 V. This indicates that increasing the surface charge density on the substrate can effectively increase the potential difference between EMR and GMR, forming deeper potential wells. When a patterned electrode is used, the electric field lines also aggregate according to the electrode pattern.

When NEF is too weak, the repelling force dominates, preventing the negative electrode from guiding particle deposition to form a pattern. With the increase in negative voltage, the NEF is enhanced, leading to the formation of the electrode pattern on the substrate. However, when the NEF is excessively strong, the repelling force from the out-electrode region dominates the motion of particles, blurring the deposited pattern.

To validate this hypothesis, an experiment using a copper cube substrate as the negative electrode (Fig. 2(a)) is conducted, with −4 kV to −10 kV voltages used to guide particle deposition on the glass slide surface. The deposited edge patterns are shown in Fig. 2(d). It can be observed contrast of space mapping region (SMR) and electrode mapping region (EMR) increases when negative voltage increases from −4 kV to −8 kV, while the contrast decreases at −10 kV. The fluorescent images of the EMR and SMR are shown in Fig. 2(b and c), which show the particle density difference between the two regions. Moreover, the fluorescent intensity along the white arrow shown in Fig. 2(d) is calculated and shown in Fig. 2(e). A similar situation occurs at the edge of the particulate pattern (Fig. S2). The variation of edge gradient with negative voltage well matches the prediction above and the optimal negative pressure for the glass slide used in this work is −8 kV, which is used in the following work.

3.2. *Influence of negative relief-patterned electrode on microparticle deposition*

As the cathode voltage transfers to the substrate surface through the filler material, changing the filler material between the cathode and substrate controls the strength of the negative electric field and thus the amount of particle deposition. Good conductors transfer potential to the substrate surface almost without loss, whereas insulators weaken the negative electric field. Additionally, different insulators have varying dielectric constants, which characterize their polarization properties in an electrostatic field, affecting the electric field differently. Based on

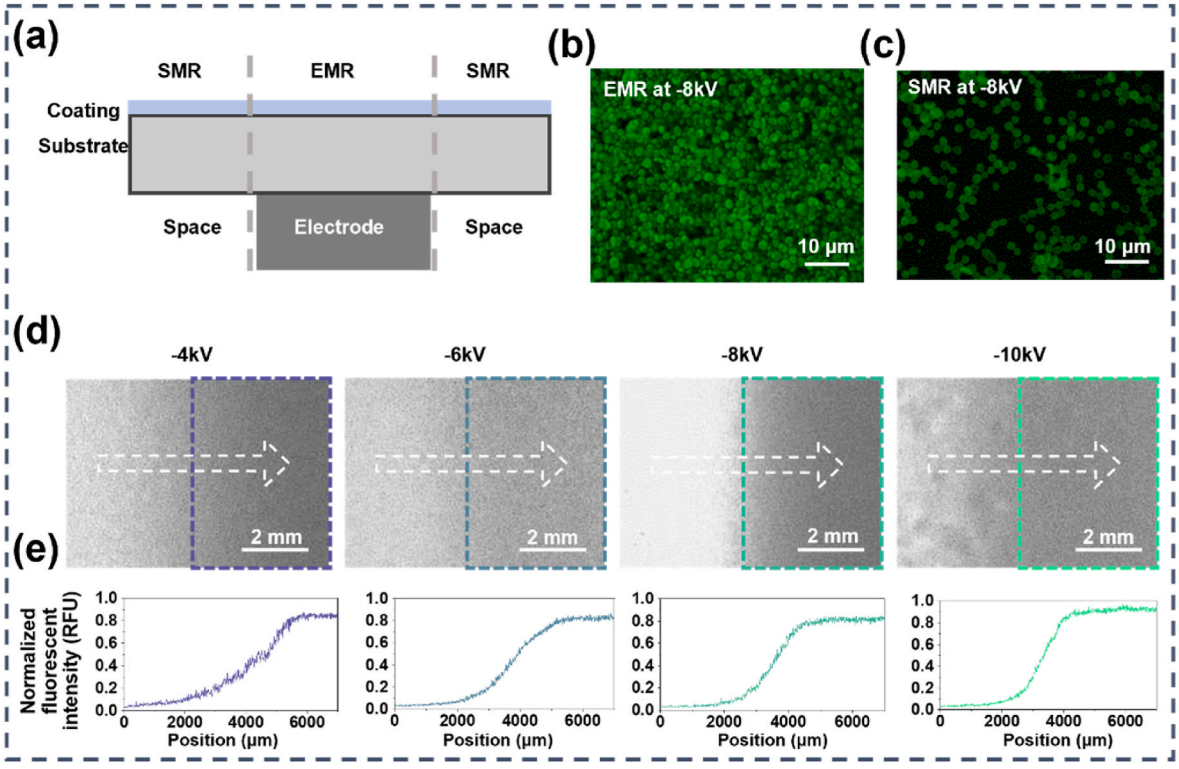

Fig. 2. The influence of negative voltage on the edge gradient of deposited pattern. (a) Schematic diagram of the negative electrode substrate. (b, c) The images of the EMR and SMR of the microparticles pattern deposited using −8 kV. (d) The optical image of the edge of the microparticles pattern using different negative voltages. (e) The measured fluorescent intensity along the white arrow in (d). The fluorescent intensities were normalized to 1000 relative fluorescent units (RFU). EMR: electrode mapping region; SMR: space mapping region.

this, we tested the variation in particle deposition with different cathode filler materials, as shown in Fig. 3(a) and (b). The electrical characteristics of different fillers are presented in Fig. 3(c). The results show that conductive fillers guide a significantly larger number of particle depositions than most insulators. There are slight differences among different conductive fillers, but more substantial differences among insulators. The reason for the significant variation among insulators is likely due to the very low dielectric constant of FH1100, which

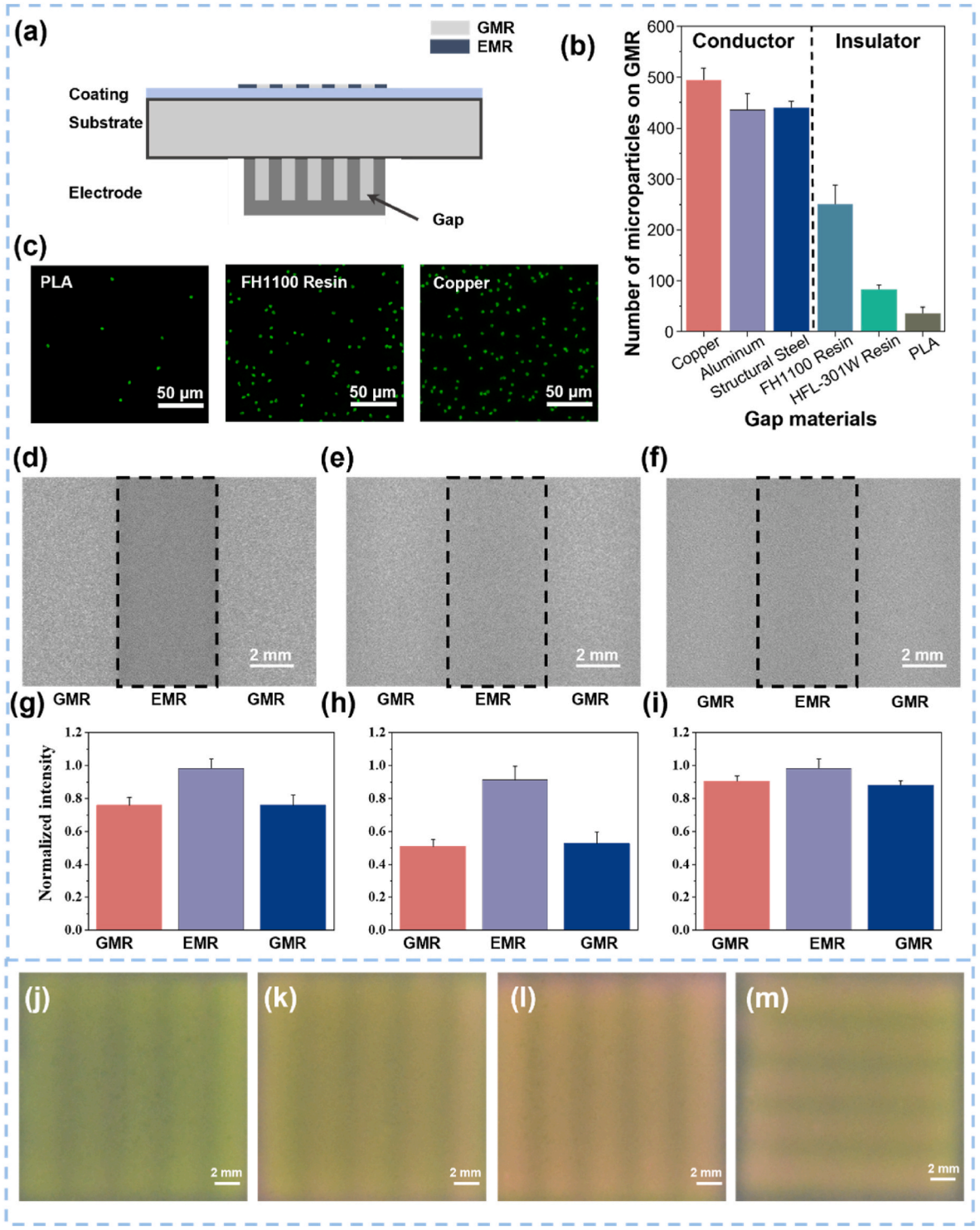

Fig. 3. Influence of electrode electric properties on microparticles deposition. (a) Schematic representation of the substrate positioned above the electrode, with intervals filled with gap material. (b) Fluorescent images depicting microparticles deposited using different electrodes with gap material. (c) The calculated number of microparticles versus the material of electrodes used for deposition. (d) Microparticles pattern deposited using an electrode with PLA as the gap material, (e) no filling, and (f) FH1100. (g–i) Normalized fluorescent intensities of different regions in (d–f), with intensities normalized to the mean intensity of the region. (j) Initial layer depicting 10 min deposition of coumarin-6 stained PLGA microparticles, followed by a second layer of (k) 5 min and (l) 10 min deposition of rhodamine B stained PLGA microparticles. (m) Double-layer cross-striped pattern deposition; the first layer shows 5 min deposition of coumarin-6 stained PLGA microparticles, followed by a second layer of 5 min deposition of rhodamine B stained PLGA microparticles.

minimally weakens the electric field, resulting in a substantially higher particle deposition compared to other insulator materials.

The variations in particle deposition quantity caused by the filler material between the cathode and substrate are used to control the contrast of deposition patterns. In this setup, different insulator blocks are placed between the striped electrodes to guide the deposition of particles into patterns of varying contrast, as shown in Fig. 3(d–i). Specifically, Fig. 3(d) and (f) use PLA and FH1100 blocks respectively to fill the gaps between electrodes, while Fig. 3(e) has no filler. By measuring the fluorescence intensity in three distinct areas in each image, we obtain the bar graphs depicted in Fig. 3(g–i). The results demonstrate that compared to the absence of a block, the PLA block significantly increases the contrast of the deposition pattern, whereas the FH1100 block noticeably reduces it. This indicates that by adjusting the structure and material composition of the cathode electrode, it is possible to programmatically control the contrast of deposition patterns, facilitating the fabrication of complex patterns.

In the CED, patterned electrodes are positioned beneath the substrate, allowing for the exchange of patterns and particle types during the deposition process. This enables the deposition of multiple layers of particles in various patterns. In our experiment, we deposited a first layer using PLGA particles containing coumarin 6, followed by a second

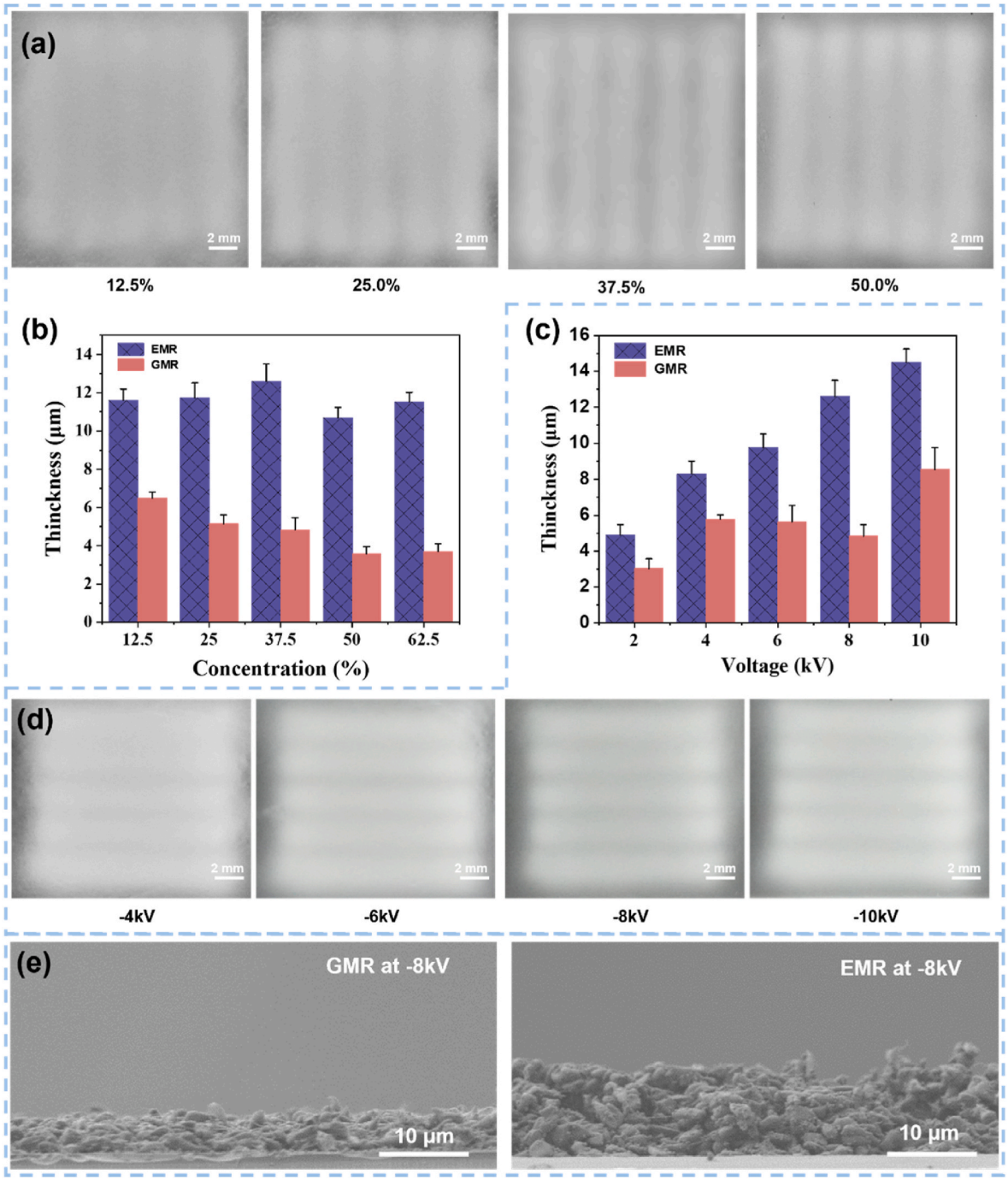

Fig. 4. Influence of coating thickness and negative electrode voltage on deposition patterns. (a) Deposition of microparticles on PVP coatings of different thicknesses. (b) EMR and GMR on different PVP coating thicknesses. (c) Thickness of EMR and GMR under different negative electrode voltages. (d) Microparticles deposition results guided by different negative electrode voltages. (e) SEM image of PLGA microparticles deposition on GMR and EMR at −8 kV.

layer of PLGA particles containing rhodamine B. Fig. 3(j–l) show the results of the second-layer particle deposition over different durations, demonstrating that the CED deposits two types of particles in varying proportions to form distinct patterns. Fig. 3(m) displays a dual-layer particle pattern with crossing stripes, proving that CED technology is capable of depositing dual-layer particles in different patterns. This showcases the potential of CED for creating complex and precise multi-layered particle depositions for advanced material and device applications. To verify the pattern of different particles, MATLAB is used to split the color image into red channel and green channel, as shown in Figs. S3 (a) and S3(b). The stripe pattern recognized and the gray value of the stripes in the red and green channels are measured and shown in Fig. S3 (c).

According to Equation (4), the thickness of the PVP coating (L_1) influences the charge dissipation in the bulk process under constant conditions of glass substrate resistivity (K_2) and thickness (L_2), as well as coating resistivity (K_1). Additionally, the potential difference $\varphi(a,t)$ influences the current density in the neutralization process.

We examine how varying the thickness of PVP coatings affects the patterns of particle deposition. Using different concentrations of PVP solution, we prepare coatings of varying thickness on glass substrates by spin coating, as depicted in Fig. S4. Under stripe electrodes, the patterns of particle deposition on different coating substrates are shown in Fig. 4 (a), which reveals that the clarity of the EMR increases with coating thickness. This enhancement is due to the weakening of charge dissipation and an increase in charge accumulation, which strengthens the potential wells on the substrate surface. The thickness differences between the EMR and the GMR of the PLGA particle layers are shown in Fig. 4(b), and the clarity of patterns, indicated by the thickness differences. As the coating thickness increases, the differences in thickness between the EMR and GMR increase, improving the clarity of the patterns. Upon exceeding a specific threshold in coating thickness, we observe that these differences cease to increase. This is attributed to the maximum charge density that the substrate surface can accommodate. This limit is associated not only with the bulk neutralization process but also with surface conduction and air neutralization. Moreover, an increase in surface charge density enhances the surface potential, thus intensifying the charge dissipation in the bulk process. Consequently, a dynamic equilibrium is reached, where the difference in thickness between the stripes and gaps no longer increases with further increases in coating thickness.

For a specific substrate, the surface potential remains unchanged once the surface charge density reaches its maximum. Subsequently, we investigate the effects of cathode voltage on deposition patterns, as shown in Fig. 4(d). The patterns become clearer, and the thickness of the stripes increases as the cathode voltage rises from 2 kV to 8 kV (Fig. 4 (c)). This is because higher cathode voltages enhance the negative electric field, which not only increases particle deposition above the electrode but also enhances potential wells, increasing the thickness difference between the EMR and GMR, thereby clarifying the patterns. However, at 10 kV, even though the particle deposition thickness increases, the difference in thickness between the EMR and GMR decreases. This reduction is due to the increased potential difference $\varphi(a, t)$, which intensifies charge dissipation in the neutralization process, affecting the surface charge density and weakening the potential wells, causing more particles to deposit in the GMR. Therefore, there is an optimal cathode voltage for a specific substrate; for a slide coated with a 37.5 % PVP solution, it is approximately 8 kV. SEM (Fig. 4(e)) shows that there is a significant difference in thickness.

Based on the above analysis, CED technology is capable of generating patterns resulting from a variety of different thicknesses and types of particle accumulation through process parameters. To demonstrate the potential of CED technology in practical applications, we have selected advanced manufacturing, cell manipulation, and antibacterial properties as application demonstrations to indicate its potential value.

3.3. Feasibility of depositing pattern containing separate islands

Patterns containing separate islands exist widely in industrial and research fields, such as the stencils of letter O. To regulate the relative position of separate parts, bridges are designed to form intact masks or excessive alignment process is required to position the mask, as shown in Fig. 5(a). However, the electrode used in CED is a relief-patterned, which has a bulk plate connects separate parts, as shown in Fig. 5(b). Thus, the pattern with separate islands could be deposited in one-step without bridges or alignment, as shown in Fig. 5(c). Hence, the CED is capable to deposit photoresist particle with complex patterns for microfluidic applications. Moreover, the patterning of the photoresist layer can dramatically decrease the waste of material during developing. As such, a pre-patterning photolithographic process is proposed in Fig. 5 (d). To evaluate the decrease of material waste, a microfluidic channel has been deposited with electrode guiding, as shown in Fig. 5(e). After developing, the channel could be recognized, and the mass of dissolved photoresist is evaluated, as shown in Fig. 5(f) and (g). Comparing with uniform deposition, the dissolved photoresist significantly decreased.

3.4. Cell adhesion with CED

Dictating cell behavior is crucial for tissue engineering and regenerative medicine. Inspired by the structure and composition of the extracellular matrix (ECM), myriad efforts have been made to engineer cell culture substrates and scaffolds with ECM-mimetic physical and biochemical properties to regulate cell behavior. In this study, in order to control cell adhesion, we create a superhydrophobic coating on glass slides by applying a layer of F127, subsequently establishing a composite electric field to control particle deposition (Fig. 6(a)). The presence of the F127 layer impedes direct cell adhesion to the glass surface. Conversely, PLGA microparticles serve as favorable sites for cell attachment, as shown in Fig. 6(b). Hence, the distribution of the PLGA microparticles could influence the distribution of the cell.

The morphological change and nuclear deformation of cells are highly correlated with cell function. Changes in nucleus size and shape, even in a transient fashion, cause chromatin reorganization and DNA methylation [33].Therefore, we examine the cell and nucleus size and deformation of endothelial cells (EA. Hy926) grown on these substrates in Fig. 6(c and d). Compared to the microparticle-free region, cell growth area by the microparticle-rich region significantly increases cell numbers, cell area and nuclear area, suggesting that physical topography can affect cell spreading (Fig. 6(e–h)). Microparticle-free region has significantly smaller cell and nuclear areas yet higher cell and nuclear aspect ratios than microparticle-rich region, where the cells randomly spread. These results indicate that these physical topographies dominantly control cell spreading area and nucleus size.

Electrospraying enables the fabrication of microparticles from a diverse range of materials. It coupled with CED technology, allows for the tailored creation of varied distributions and layer thicknesses. In future studies, we aim to develop complex and realistic three-dimensional cell culture environments by manipulating the stacking of microparticles in the layer direction. Such 3D environments are instrumental in more accurately simulating in vivo conditions, providing deeper insights into cell behavior crucial for basic biological research and drug development. By varying the height of microparticle layers, we can emulate the structural characteristics of various human tissues, such as the multilayered architecture of skin, muscle, or bone tissues. This capability holds immense potential for reconstructing damaged tissues in tissue engineering or developing artificial organs. Furthermore, the variation in microparticle layering can create distinct physical and chemical microenvironments. This is particularly pivotal in studying how cells respond to different environmental conditions and mechanical stimuli, providing valuable insights into cell-microenvironment interactions.

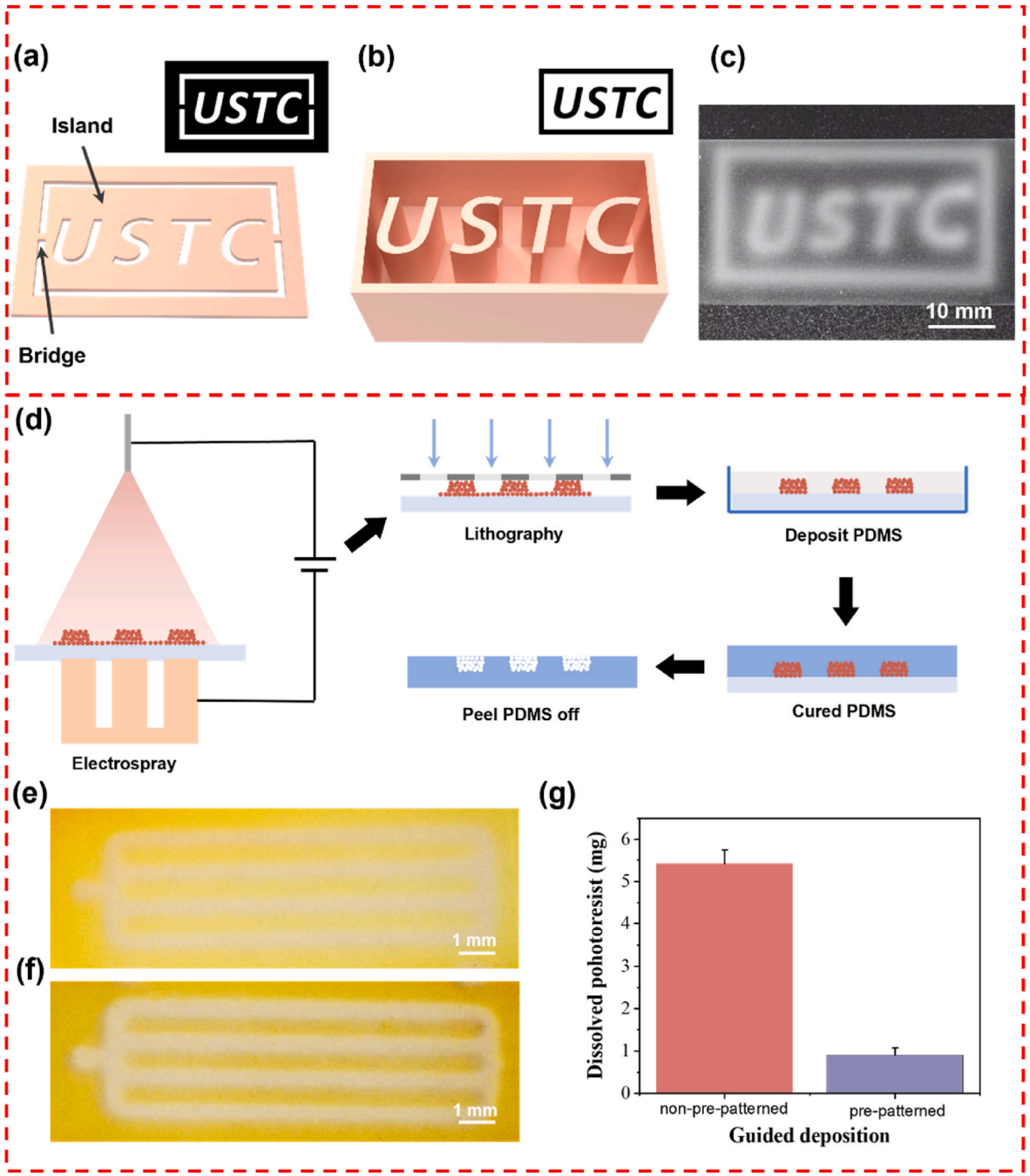

Fig. 5. The deposition of patterns with separate islands. (a) The standard mask utilized for pattern creation with segregated islands in mask-based deposition processes. (b) The electrode used for CED to deposit same pattern. (c) Deposited microparticles pattern using CED. (d) The schematic of the pre-patterning photolithographic process. (e) The pre-patterned S1813 microparticle layer. (f) The S1813 layer after exposure. (g) Dissolved photoresist for the S1813 layer, comparing pre-patterned and non-pre-patterned processes.

3.5. Customized drug-coating bandage fabricated with CED

Precision medicine, which includes tailoring drug delivery to individual needs, is a cornerstone of modern healthcare strategies [34]. For instance, malignant melanoma is notoriously challenging to remove surgically, and residual tumor cells often lead to recurrences [35,36]. Post-operative chemotherapy is typically required; however, chemotherapeutic agents like 5-fluorouracil often harm healthy tissues due to their potent side effects [37].Thus, the careful design of drug delivery regions and the precise control over drug distribution across different areas are essential prerequisites for achieving precision in medication administration.

In this work, curcumin-laden PLGA microparticles as the model drug are used for the demonstration. Curcumin is a naturally occurring molecule that has been shown to possess antioxidant, antibacterial, and anti-inflammatory properties, as well as demonstrating excellent anti-tumor properties by inhibiting the proliferation of various tumor cells and lowering tumor-associated transcription factors [38–40]. The use of curcumin in this context serves to illustrate the potential of our drug delivery platform. It showcases its capability to effectively encapsulate and release a bioactive molecule with diverse therapeutic functions, thereby validating the concept of our microparticle system.

The curcumin-laden microparticles are deposited on a medical bandage under the guidance of a circular electrode. After deposition, the

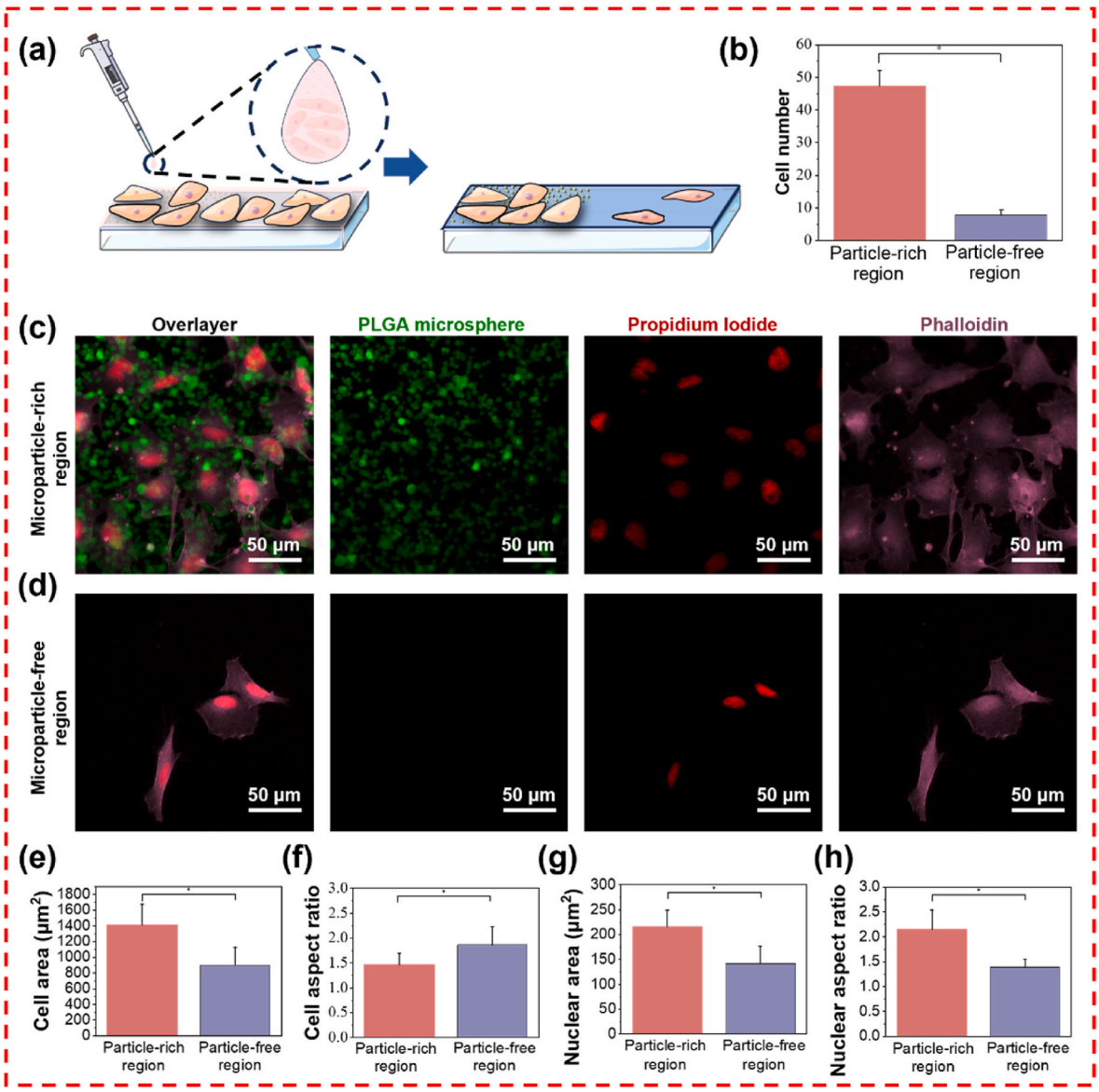

Fig. 6. Control of cell distribution using CED. (a) Schematic representation illustrating the influence of particles on cell adhesion. (b) Comparison of cell numbers on substrates with particle-rich region and particle-free region. (c, d) Representative immunofluorescence images of endothelial cells (EA. Hy926) cultured on microparticle-free and microparticle-rich substrates, respectively. F-actin fibers were visualized using phalloidin staining, nuclei were counterstained with Propidium Iodide, and PLGA microspheres were marked in green. Quantitative analysis of cell area (e), cell aspect ratio (f), nucleus area (g), and nucleus aspect ratio (h) in endothelial cells (EA. Hy926) across different conditions. Elongation is expressed as the aspect ratio of cells and nuclei. *: $p < 0.05$.

medication on the bandage can match the lesion on the skin, as shown in Fig. 7(a). During the electrospray fabrication process, microparticles were formulated with 5 % PLGA as the matrix material and 5 % curcumin, achieving a consistent drug loading efficiency of 50 %. This composition successfully yielded microparticles with an average size of 2.56 ± 0.35 μm (Fig. S5). This achievement confirms the successful synthesis of curcumin-loaded PLGA microparticles. In this formulation, the high molecular weight of PLGA functions primarily as a structuring agent, crucial in shaping the microparticles' architecture. Furthermore, the slow biodegradation rate of PLGA in the body enables these drug-laden microparticles to facilitate sustained release, progressively administering the encapsulated curcumin over an extended duration. This characteristic renders them exceptionally well-suited for applications that demand controlled drug delivery. The drug release profiles of particles outer and inner electrode regions were tested *in vitro* and shown in Fig. 7(b), which gives a significant difference of total dose between the two regions. It indicates the release characteristics of the drug are determined by the parameters governing deposition, thereby ensuring controlled release profiles of the drug. Furthermore, the release of curcumin is examined in an antimicrobial assay to verify that the model drug was released effectively. In Fig. 7(c), the survival bacteria colony shows significant difference between different groups, which means that different antibacterial properties could be achieved using CED coated bandage. This was further evidenced by the fluorescent images of dyed bacteria (Fig. 7(d)) and the calculated colony forming units (Fig. 7(e)). Through drug release tests and antimicrobial tests, it has been shown that the CED can effectively control the amount of deposition in different areas. In addition, although the deposition of electrospray particles hinders the adhesion of the adhesive portion of the tape, it does not affect its normal use, similar to a band-aid.

This article primarily showcases the use of CED to guide microparticle deposition. Electrospray, a well-established method for microsphere fabrication, utilizes not only oil-soluble materials like PLGA but also water-soluble substances such as sodium alginate and PVA, both of

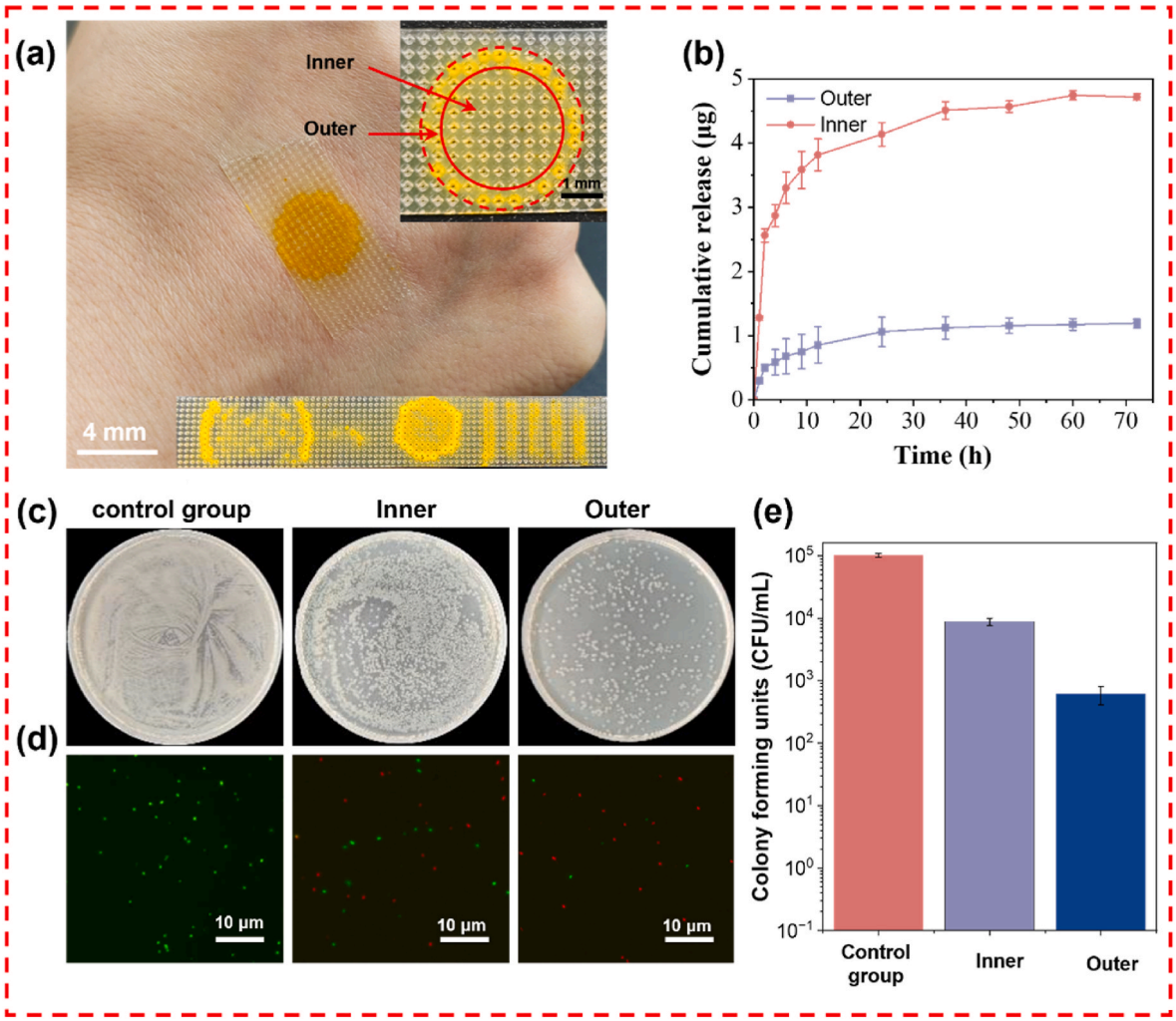

Fig. 7. Customized fabrication of antibacterial bandage using CED. (a) A curcumin loaded antibacterial bandage used for the treatment of skin infection. The inset shows the contrast pattern on bandage. The solid line circles the electrode region while the dash line circles the spread of particles. (b) The cumulative release of curcumin of different regions. (c) The cultured bacteria before and after antibacterial test. (d) The fluorescent images of dyed bacteria. (e) Calculated colony forming units (CFU) per mL after culturing.

which are adept at encapsulating drugs, facilitating controlled release [41–43]. In future, combining electrospray with CED will enable the production of slow-release microcapsules while allowing for customized drug delivery on bandages, which is beneficial for precision medicine in transdermal drug delivery [44]. Moreover, the CED can precisely control the distribution and quantity of particles generated through electrospray, allowing for the adjustment of drug delivery range and concentration, thus reducing the impact of drugs on normal tissues. Additionally, The CED permits the deposition of multiple layers of drug-laden microparticles on a substrate, enabling the bandage to deliver various drugs, simultaneously for optimal therapeutic outcomes.

Our research primarily concentrated on the electrical properties of substrate materials, which are crucial for effective electric-field-guided deposition. This emphasis was driven by our initial experimental design, which aimed to establish a fundamental understanding of the electrostatic interactions essential for pattern formation. While we recognized the pivotal role of resistance, other substrate characteristics such as surface roughness and chemical stability were not sufficiently emphasized in our analysis. It is now clear that variations in these substrate characteristics can significantly impact the quality and precision of deposition patterns. The current limitations of our technique—such as efficiency issues, non-sharp boundaries, and dependence on substrate material—restrict its broader applicability, particularly in contexts requiring precise and clear boundaries. To address these challenges and enhance the method's reliability and adaptability for practical applications, future work will extend our research to include a wider range of substrate materials. Specifically, we will target substrates commonly used in applications like tissue engineering scaffolds, such as PMMA and PLA, to thoroughly explore how different substrate properties affect deposition quality. By tailoring our approach to meet specific application needs, we aim to refine particle deposition and improve pattern fidelity, thereby aligning our methodology more closely with the requirements of advanced material applications.

All in all, we have successfully validated the principles and optimized the parameters of the Combinatory Electric-field-guided Deposition (CED) at a laboratory scale. Therefore, scaling up the CED to an industrial level holds significant practical importance. The efficiency of a single nozzle is currently low, which poses a challenge in transitioning from laboratory scale to industrial production. Increasing the number of nozzles and expanding the size of electrodes can effectively enhance the efficiency of particle production. Moreover, the electrospray process often involves the evaporation of organic solvents, particularly under high voltage conditions. The primary use of acetone could also pose potential safety risks. In our future work, optimizing experimental protocols and adopting safer solvents will be key focuses. Overall, CED demonstrates enormous potential across various fields, from material

science to biomedicine, showcasing broad market demand. We remain optimistic about the breakthroughs this will achieve in practical applications and are committed to continuing its industrialization process.

4. Conclusions

In this study, we develop the combinatory electric-field-guided deposition (CED) technology, which can assemble microparticles onto multiple substrates with pre-defined patterns. Unlike the conventional electrospray-based patterning methods that place a mask upon the substrate or sputter electrode to alter the substrate, CED positions patterned electrode beneath the substrate. This configuration minimizes the influence of the morphology and surface property of the substrate in particle patterning. Additionally, the process allows for easy switching of substrates or electrodes, enabling the deposition of multi-layered patterns with varying designs. Moreover, CED utilizes a relief-like electrode, eliminating the need for bridges to connect islands in patterns featuring separate islands, which is necessary for the mask or electrode-based methods. Besides, the electrical properties of the electrode, which influence the deposition profile of particles, can be utilized to adjust the contrast of a particulate pattern. In forthcoming studies, we aim to delve deeper into selective deposition under varying electrode parameters to attain grayscale patterning of particles. We anticipate that CED could find widespread applications in various fields. For instance, it facilitates the development of programmable drug delivery systems capable of delivering drugs with complex release patterns. Additionally, it controls the patterning of cell distribution, thereby providing more effective solutions for regenerative medicine and tissue repair by accurately controlling the distribution of cells in artificially constructed tissues and organs.

CRediT authorship contribution statement

Zhiyuan Zheng: Writing – original draft, Visualization, Methodology, Funding acquisition, Data curation, Conceptualization. **Yang Zhang:** Methodology. **Jinyu Xing:** Software. **Xin Li:** Resources. **Zhiqiang Zhu:** Visualization. **Min Ye:** Writing – review & editing, Writing – original draft, Conceptualization. **Shuwei Shen:** Writing – review & editing. **Ronald X. Xu:** Writing – review & editing.

Declaration of competing interest

The authors declare that they have no known competing financial interests or personal relationships that could have appeared to influence the work reported in this paper.

Data availability

Data will be made available on request.

Acknowledgements

The authors are grateful for microfabrication support from Wei Xu (Advanced Manufacturing Platform at Suzhou Institute for Advanced Research of USTC). This work was supported by the National Key R&D Program of China [grant numbers 2021YFC2401402, 2022YFA1104802, 2022YFA1104803] and Postdoctoral Research Funding of Anhui Province of China (Grant No. 2022B658).

Appendix A. Supplementary data

Supplementary data to this article can be found online at https://doi.org/10.1016/j.mtbio.2024.101207.

References

[1] M.S. Chen, S.L. Brandow, T.L. Schull, D.B. Chrisey, W.J. Dressick, A non-covalent approach for depositing spatially selective materials on surfaces, Adv. Funct. Mater. 15 (8) (2005) 1364–1375.
[2] J.A. Phillippi, E. Miller, L. Weiss, J. Huard, A. Waggoner, P. Campbell, Microenvironments engineered by inkjet bioprinting spatially direct adult stem cells toward muscle-and bone-like subpopulations, Stem cells 26 (1) (2008) 127–134.
[3] C.P. Tan, H.G. Craighead, Surface engineering and patterning using parylene for biological applications, Materials 3 (3) (2010) 1803–1832.
[4] V.H. Nguyen, J. Resende, C. Jiménez, J.-L. Deschanvres, P. Carroy, D. Munoz, D. Bellet, D. Munoz-Rojas, Deposition of ZnO based thin films by atmospheric pressure spatial atomic layer deposition for application in solar cells, J. Renew. Sustain. Energy 9 (2) (2017) 021203.
[5] D.J. Collins, R. O'Rorke, A. Neild, J. Han, Y. Ai, Acoustic fields and microfluidic patterning around embedded micro-structures subject to surface acoustic waves, Soft Matter 15 (43) (2019) 8691–8705.
[6] S. Yuan, F. Lei, Z. Liu, Q. Tong, T. Si, R.X. Xu, Coaxial electrospray of curcumin-loaded microparticles for sustained drug release, PLoS One 10 (7) (2015) e0132609.
[7] E. Koos, Capillary suspensions: particle networks formed through the capillary force, Curr. Opin. Colloid Interface Sci. 19 (6) (2014) 575–584.
[8] G.M. Whitesides, B. Grzybowski, Self-assembly at all scales, Science 295 (5564) (2002) 2418–2421.
[9] R. Hölzel, Single particle characterization and manipulation by opposite field dielectrophoresis, J. Electrost. 56 (4) (2002) 435–447.
[10] Z. Huang, Z. Wu, P. Wang, T. Zhou, L. Shi, Z. Liu, J. Huang, Multi-particle interaction in AC electric field driven by dielectrophoresis force, Electrophoresis 42 (21–22) (2021) 2189–2196.
[11] A. Winkleman, B.D. Gates, L.S. McCarty, G.M. Whitesides, Directed self-assembly of spherical particles on patterned electrodes by an applied electric field, Advanced materials 17 (12) (2005) 1507–1511.
[12] J. Berthier, Chapter 6 - introduction to liquid Dielectrophoresis**This chapter has been written with the collaboration of raphaël renaudot and vincent agache, CEA-LETI, in: J. Berthier (Ed.), Micro-Drops and Digital Microfluidics (second ed.), William Andrew Publishing2013, pp. 303-324.
[13] A.A. Kava, C.S. Henry, Exploring carbon particle type and plasma treatment to improve electrochemical properties of stencil-printed carbon electrodes, Talanta 221 (2021) 121553.
[14] K. Koh, H. Hwang, C. Park, J.Y. Lee, T.Y. Jeon, S.-H. Kim, J.K. Kim, U. Jeong, Large-area accurate position registry of microparticles on flexible, stretchable substrates using elastomer templates, ACS applied materials & interfaces 8 (41) (2016) 28149–28158.
[15] W.-C. Yan, J. Xie, C.-H. Wang, Electrical field guided electrospray deposition for production of gradient particle patterns, ACS applied materials & interfaces 10 (22) (2018) 18499–18506.
[16] D. Lowke, D. Talke, I. Dressler, D. Weger, C. Gehlen, C. Ostertag, R. Rael, Particle bed 3D printing by selective cement activation–Applications, material and process technology, Cement Concr. Res. 134 (2020) 106077.
[17] B.D. Myers, E. Palacios, D.I. Myers, S. Butun, K. Aydin, V.P. Dravid, Stimuli-Responsive DNA-linked nanoparticle arrays as programmable surfaces, Nano Lett. 19 (7) (2019) 4535–4542.
[18] A.J. Vargas, C.C. Harris, Biomarker development in the precision medicine era: lung cancer as a case study, Nat. Rev. Cancer 16 (8) (2016) 525–537.
[19] M. Arnedos, C. Vicier, S. Loi, C. Lefebvre, S. Michiels, H. Bonnefoi, F. Andre, Precision medicine for metastatic breast cancer—limitations and solutions, Nat. Rev. Clin. Oncol. 12 (12) (2015) 693–704.
[20] W. Sun, X. Liang, J. Lei, C. Jiang, D. Sheng, S. Zhang, X. Liu, H. Chen, Regulating cell behavior via regional patterned distribution of heparin-like polymers, Biomater. Adv. 154 (2023) 213664.
[21] H. Che, M. Selig, B. Rolauffs, Micro-patterned cell populations as advanced pharmaceutical drugs with precise functional control, Adv. Drug Deliv. Rev. 184 (2022) 114169.
[22] K. Higashi, K. Uchida, A. Hotta, K. Hishida, N. Miki, Micropatterning of silica nanoparticles by electrospray deposition through a stencil mask, J. Lab. Autom. 19 (1) (2014) 75–81.
[23] J. Garra, T. Long, J. Currie, T. Schneider, R. White, M. Paranjape, Dry etching of polydimethylsiloxane for microfluidic systems, J. Vac. Sci. Technol. A: Vacuum, Surfaces, and Films 20 (3) (2002) 975–982.
[24] E.P. Yalcintas, K.B. Ozutemiz, T. Cetinkaya, L. Dalloro, C. Majidi, O.B. Ozdoganlar, Soft electronics manufacturing using microcontact printing, Adv. Funct. Mater. 29 (51) (2019) 1906551.
[25] Z. Xin, Y. Liu, X. Li, S. Liu, Y. Fang, Y. Deng, C. Bao, L. Li, Conductive grid patterns prepared by microcontact printing silver nanoparticles ink, Mater. Res. Express 4 (1) (2017) 015021.
[26] B. Zhang, G. Zhang, Interpretation of the surface charge decay kinetics on insulators with different neutralization mechanisms, J. Appl. Phys. 121 (10) (2017).
[27] H. Hama, T. Hikosaka, S. Okabe, H. Okubo, Cross-equipment study on charging phenomena of solid insulators in high voltage equipment, IEEE Trans. Dielectr. Electr. Insul. 14 (2) (2007) 508–519.
[28] P. Llovera, P. Molinie, New methodology for surface potential decay measurements: application to study charge injection dynamics on polypropylene films, IEEE Trans. Dielectr. Electr. Insul. 11 (6) (2004) 1049–1056.

[29] I.W. McAllister, Decay of charge deposited on the wall of gaseous void, IEEE Trans. Electr. Insul. 27 (6) (1992) 1202–1207.
[30] E. Baum, T. Lewis, R. Toomer, The lateral motion of charge on thin films of polyethylene terephthalate, J. Phys. Appl. Phys. 11 (6) (1978) 963.
[31] G. Chen, A new model for surface potential decay of corona-charged polymers, J. Phys. Appl. Phys. 43 (5) (2010) 055405.
[32] Y. Zhu, P.R. Chiarot, Surface charge accumulation and decay in electrospray printing, J. Phys. Appl. Phys. 54 (7) (2020) 075301.
[33] Y. Song, J. Soto, B. Chen, T. Hoffman, W. Zhao, N. Zhu, Q. Peng, L. Liu, C. Ly, P. K. Wong, Transient nuclear deformation primes epigenetic state and promotes cell reprogramming, Nat. Mater. 21 (10) (2022) 1191–1199.
[34] E.A. Ashley, Towards precision medicine, Nat. Rev. Genet. 17 (9) (2016) 507–522.
[35] H. Helgadottir, I. Rocha Trocoli Drakensjö, A. Girnita, Personalized medicine in malignant melanoma: towards patient tailored treatment, Front. Oncol. 8 (2018) 202.
[36] S. Salmon, Kinetics of Minimal Residual Disease, Adjuvant Therapies and Markers of Post-Surgical Minimal Residual Disease I, Springer1979, pp. 5-15.
[37] W. She, K. Luo, C. Zhang, G. Wang, Y. Geng, L. Li, B. He, Z. Gu, The potential of self-assembled, pH-responsive nanoparticles of mPEGylated peptide dendron–doxorubicin conjugates for cancer therapy, Biomaterials 34 (5) (2013) 1613–1623.
[38] B. Saifi, S.M. Haftcheshmeh, M. Feligioni, E. Izadpanah, K. Rahimi, K. Hassanzadeh, A. Mohammadi, A. Sahebkar, An overview of the therapeutic effects of curcumin in reproductive disorders with a focus on the antiinflammatory and immunomodulatory activities, Phytother Res 36 (2) (2022) 808–823.
[39] A.J. Abadi, S. Mirzaei, M.K. Mahabady, F. Hashemi, A. Zabolian, F. Hashemi, P. Raee, S. Aghamiri, M. Ashrafizadeh, A.R. Aref, Curcumin and its derivatives in cancer therapy: potentiating antitumor activity of cisplatin and reducing side effects, Phytother Res. 36 (1) (2022) 189–213.
[40] M. Urošević, L. Nikolić, I. Gajić, V. Nikolić, A. Dinić, V. Miljković, Curcumin: biological activities and modern pharmaceutical forms, Antibiotics 11 (2) (2022) 135.
[41] S. Song, Z. Li, J. Li, Y. Liu, Z. Li, P. Wang, J. Huang, Electrospray Nano-Micro Composite Sodium Alginate Microspheres with Shape-Adaptive, Antibacterial, and Angiogenic Abilities for Infected Wound Healing, ACS Appl Mater Interfaces 16 (22) (2024) 28147–28161.
[42] J. Li, J. Wang, J. Li, X. Yang, J. Wan, C. Zheng, Q. Du, G. Zhou, X. Yang, Fabrication of Fe3O4@ PVA microspheres by one-step electrospray for magnetic resonance imaging during transcatheter arterial embolization, Acta Biomater. 131 (2021) 532–543.
[43] Z. Zheng, S. Shen, H. Shi, P. Yao, Z. Zhu, C. Zhang, S. Zhang, X. Hu, R.X. Xu, Rational engineering of dual Drug-Formulated multifunctional microneedles to accelerate in vivo cutaneous infection treatment, Chem. Eng. J. (2024) 154076.
[44] M.T. Manzari, Y. Shamay, H. Kiguchi, N. Rosen, M. Scaltriti, D.A. Heller, Targeted drug delivery strategies for precision medicines, Nat. Rev. Mater. 6 (4) (2021) 351–370.